Inorganic Chemistry

Article

pubs.acs.org/IC

Mechanism of Magnetostructural Transitions in Copper-Nitroxide-Based Switchable Molecular Magnets: Insights from ab Initio Quantum Chemistry Calculations

Julie Jung,[†,‡] Boris Le Guennic,[‡] Matvey V. Fedin,[§] Victor I. Ovcharenko,[§] and Carmen J. Calzado*[,†]

[†]Departamento de Química Física, Universidad de Sevilla, Sevilla, Spain

[‡]Institut des Sciences Chimiques de Rennes, UMR 6226 CNRS, Université de Rennes 1, 263 Avenue du Général Leclerc, 35042 Cedex Rennes, France

[§]International Tomography Center, Siberian Branch of Russian Academy of Science and Novosibirsk State University, 630090 Novosibirsk, Russia

Supporting Information

ABSTRACT: The gradual magnetostructural transition in breathing crystals based on copper(II) and pyrazolyl-substituted nitronyl nitroxides has been analyzed by means of DDCI quantum chemistry calculations. The magnetic coupling constants (J) within the spin triads of $Cu(hfac)_2L^{Bu}\cdot 0.5C_8H_{18}$ have been evaluated for the X-ray structures reported at different temperatures. The coupling is strongly antiferromagnetic at low temperature and becomes ferromagnetic when the temperature increases. The intercluster magnetic coupling (J') is antiferromagnetic and shows a marked dependence on temperature. The magnetostructural transition can be reproduced using the calculated J values for each structure in the simulation of the magnetic susceptibility. However, the μ(T) curve can be improved nicely by considering the coexistence of two phases in the transition region, whose ratio varies with temperature corresponding to both the weakly and strongly coupled spin states. These results complement a recent VT-FTIR study on the parent $Cu(hfac)_2L^{Pr}$ compound with a gradual magnetostructural transition.

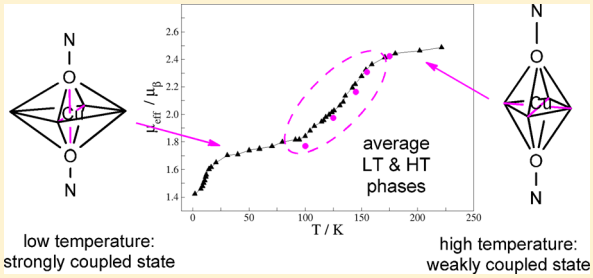

1. INTRODUCTION

Research on molecular magnetism continues drawing significant attention in materials science with single-molecule magnets and switchable magnetoactive compounds being most intensively investigated.[1−7] Spin crossover (SCO) and related phenomena were the topics of many studies aimed at the development of magnetic switches for potential applications in spintronics.[6,7] In addition to classical SCO compounds, a large family of heterospin polymer-chain complexes of Cu(II) hexafluoroacetylacetonate ($Cu(hfac)_2$) with pyrazolyl-substituted nitronyl nitroxides L^R (R = Me, Et, Pr, Bu) has been synthesized and characterized (Figure 1).[8−22]

These $Cu(hfac)_2L^R$ systems exhibit SCO-like magnetic anomalies that can be thermally and optically induced, in many aspects similar to classical spin crossover, but different in nature. The crystal undergoes reversible structural rearrangements, accompanied by changes of the exchange interaction between Cu(II) and the nitroxide spins in the spin triad when the temperature changes. At high temperatures, the spins are weakly ferromagnetically coupled (weakly exchange-coupled state, WS), whereas at low temperatures, Cu(II) and nitroxide spins are coupled by a strong antiferromagnetic interaction, and the spin triad converts to the strongly coupled spin state (strongly exchange-coupled state, SS) with a total spin of $S = 1/2$. As a result, the effective magnetic moment μ_{eff} decreases when the temperature drops. The change in the magnetic moment $\Delta\mu_{eff}$ can be gradual or abrupt. Because the spin transition occurs with a significant change in the unit cell

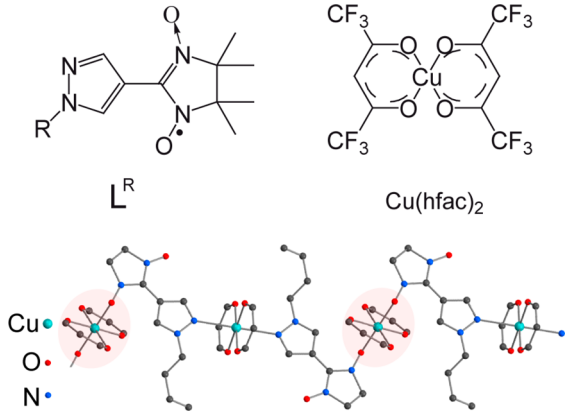

Figure 1. Chemical structure of nitronyl nitroxide (L^R) and $Cu(hfac)_2$ (top) and head-to-head polymer-chain structure of breathing crystals exemplified using $Cu(hfac)_2L^{Bu}$ (bottom); Cu centers involved in spin triads are circled.

Received: April 8, 2015
Published: June 30, 2015

DOI: 10.1021/acs.inorgchem.5b00794
Inorg. Chem. 2015, 54, 6891−6899

volume, these systems have been called *breathing crystals*. Similar magnetic anomalies have also been reported for other compounds containing copper/nitroxide heterospins that are magnetically coupled.[23−33]

$Cu(hfac)_2L^R$ breathing crystals have been experimentally investigated by means of many techniques, including SQUID magnetometry, X-ray diffraction (XRD), electron paramagnetic resonance (EPR), and optical techniques.[8,9,21,22] The magnetic anomalies have been attributed to a significant change of the magnetic (exchange) interactions (J) within the spin triads with temperature.[11] However, each of the experimental techniques has limitations for studying magnetostructural transitions in breathing crystals. For instance, SQUID magnetometry reports bulk magnetic properties of the sample, and if different kinds of paramagnetic centers are present, the analysis is not immediately straightforward. XRD allows one to monitor structural changes and make only order-of-magnitude estimates of exchange interactions; optical spectroscopies likewise provide only indirect information on exchange interactions. In this sense, EPR is a more suitable technique for studying magnetic anomalies in breathing crystals, and it was indeed intensively used for characterization of exchange interactions in spin triads and their thermally/photoinduced changes.[9] However, in a number of situations, its sensitivity is still limited, in particular when appreciable intermolecular (intercluster) exchange couplings are present.

In this context, the development and application of advanced theoretical approaches for evaluation of exchange interactions based on XRD structure is very topical, and new insights based on precisely calculated J values relative to temperature/structure would be of great aid. At present, theoretical studies of breathing crystals are relatively scarce, and most of them are preliminary. Some of these studies employ elastic-type theories and are not focused on precise calculation of exchange interactions based on the crystal structures.[34−36] In some others, the exchange coupling within the spin triad has been calculated by means of broken-symmetry DFT calculations[10] for solvates of $Cu(hfac)_2L^{Bu}$ and for isolated groups of nitronyl nitroxide to estimate the interchain couplings.[14] The resulting J values do not reproduce the experimental data well.[10] Also, a theoretical study based on CASPT2 calculations has been reported where the magnetic coupling constants and g factors within the spin triad in $Cu(hfac)_2L^{Pr}$ have been evaluated at low and high temperatures.[37] The results are strongly dependent on the zeroth-order Hamiltonian chosen in the perturbative approach, and thus, they only provide a qualitative description of the thermal dependence of the magnetic moment. Regarding the periodic treatment, it is worth mentioning a recent study by Streltsov et al.[38] where the band structure of a related head-to-tail $Cu(hfac)_2L^R$ polymer chain has been analyzed.

Therefore, the aim of this work is to apply state-of-the-art quantum chemistry approaches for the evaluation of exchange interactions in breathing crystals. Below, we use wave function methods, mainly the difference dedicated configuration interaction (DDCI) approach,[39] for representative compound $Cu(hfac)_2L^{Bu}\cdot 0.5C_8H_{18}$, whose magnetic and structural properties are known from the literature,[10,11] to evaluate intra- and intercluster exchange interaction constants and their evolution with temperature. The results allow for intepretation of the molecular mechanism and magnetostructural correlations governing the gradual transition in $Cu(hfac)_2L^{Bu}\cdot 0.5C_8H_{18}$.

2. EXPERIMENTAL SECTION

The $Cu(hfac)_2L^{Bu}\cdot 0.5C_8H_{18}$ complex consists of polymeric chains with a head-to-head motif, leading to the formation of three-spin nitroxide-copper(II)-nitroxide clusters alternated with one-spin magnetically isolated copper(II) units along the chain (Figure 1). The chains are magnetically connected through the interaction provided by the terminal nitroxide groups of the three-spin clusters of two neighboring chains. This intercluster interaction gives 1D exchange channels that do not coincide with the polymeric chains but rather spread across them.[14]

The calculations provide estimates of the magnetic coupling constants within the three-spin cluster (intracluster exchanges) and between the clusters (intercluster exchange). The triads contain three magnetic centers with $S = 1/2$: two nitronyl nitroxide groups and one Cu(II) ion between them (Figure 2). All of the calculations have been performed on the basis of the X-ray data provided for $Cu(hfac)_2L^{Bu}$ with octane as the solvent.[10] To reduce the computational cost, we replaced the external ligands of the spin triad, including the pyrazolyl rings, CH_3 groups in nitronyl nitroxide ligand, and CF_3 groups of hfac, by H atoms (Figure 2). A fixed C−H distance of 0.88 Å is employed for the H replacing the CF_3 groups and 0.93 Å for the H replacing the pyrazolyl and CH_3 groups. Despite the simplifications, the resulting model preserves the geometrical features of the three active centers in such a way that the effect of the modeling on the amplitude of the J values is expected to be small if any. ANO-RCC-type basis functions[40] have been employed for all of the atoms with contractions [6s5p3d2f] for Cu, [4s3p2d] for N and O in nitronyl nitroxide groups and for C atoms bridging two NO groups,[41] [4s3p] for the rest of C and O, and [2s] for all hydrogen atoms. The Cholesky decomposition implemented in the Molcas 7.8 code[42] was used to generate the list of the two electron integrals in all of the calculations. The same code was used to obtain the CASSCF MOs. DDCI calculations have been performed by means of the CASDI code[43] with an energy convergence threshold of 10^{-7} atomic units.

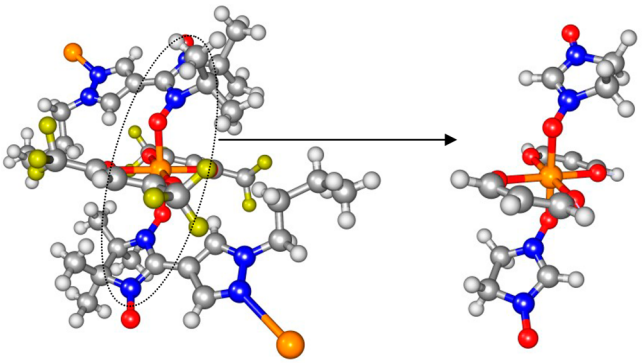

Figure 2. Real (left) and model (right) spin triad in the 100 K structure. Cu, O, N, C, F, and H are represented by orange, red, blue, dark gray, yellow, and light gray, respectively.

3. RESULTS AND DISCUSSION

3.1. Evaluation of the Intracluster Magnetic Coupling Constants. The variable temperature magnetic data for the triad can be interpreted on the basis of an isotropic Heisenberg behavior with three $S = 1/2$ centers and two types of interactions between them. J corresponds to the interaction between the NO groups and the Cu center, and J_{NO} is the coupling between the two NO groups, such that

$$\hat{H} = -2J(\hat{S}_{NO1}\hat{S}_{Cu} + \hat{S}_{NO2}\hat{S}_{Cu}) - 2J_{NO}\hat{S}_{NO1}\hat{S}_{NO2} \quad (1)$$

DOI: 10.1021/acs.inorgchem.5b00794
Inorg. Chem. 2015, 54, 6891−6899

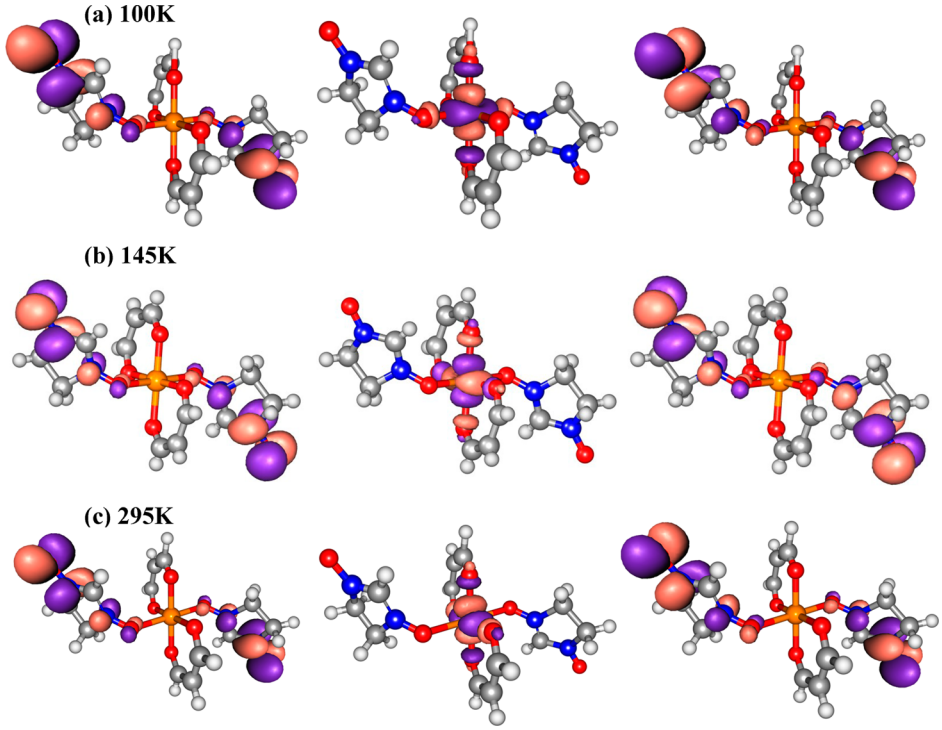

Figure 3. Active orbitals for the quartet CASSCF(3/3) wave function obtained from the structures at 100 K (top), 145 K (middle), and 295 K (bottom).

This Hamiltonian has three eigenvalues corresponding to two doublet states of symmetry A_g and A_u, D_1 and D_2, respectively, and a quartet of symmetry A_u, Q_2

$$E(D_2) = 3J$$
$$E(D_1) = J + 2J_{NO}$$
$$E(Q_2) = 0 \quad (2)$$

Then, it is possible to evaluate J and J_{NO} from the energies of the three magnetic states.

In this work, the energy of these states is determined by means of difference dedicated configuration interactions (DDCI) calculations,[39] considered as a reference method for the evaluation of magnetic coupling constants (for instance, see citations in ref 44). DDCI is a multiconfigurational reference approach including dynamic correlation at a variational level. In this approach, a minimal complete active space (CAS) wave function (with all possible distributions of the unpaired electrons over the magnetic orbitals) is employed as reference, and a CI matrix is built by adding all singly and doubly excited determinants involving at least one of the active orbitals. In the spin triad, the three unpaired electrons are essentially localized on three molecular orbitals, resulting from the linear combination of the π orbitals of the nitronyl nitroxide groups and the singly occupied Cu 3d orbital. This gives an active space with 3 electrons in 3 orbitals, CAS(3/3). In this approach, the DDCI energy and wave function of all the magnetic states are calculated with a common set of MOs. Two sets of molecular orbitals have been employed, as obtained from CASSCF(3/3) calculations on the D_2 and Q_2 states. The results are almost independent of the choice of the MOs. The active magnetic orbitals resulting from a CASSCF(3/3) calculation on the Q_2 state are shown in Figure 3 for the 100 K (top), 145 K (middle), and 295 K (bottom) structures. Similar shapes are found for the orbitals resulting from the D_2 CASSCF(3/3) wave function. The active orbitals are very similar for both structures, the main difference is related to the magnetic orbital centered on the metal atom. The active Cu 3d orbital is placed in the equatorial plane in both structures, but because the Cu Jahn−Teller axes are distinct at 100 and 295 K, this plane is oriented differently. At low temperature, the equatorial plane contains the oxygen atoms of the bridging NO groups, whereas at high temperature, the equatorial plane contains the four oxygen atoms of the *hfac* groups and a negligible/null overlap with the nitronyl nitroxide orbitals.

The J values resulting from the energy differences obtained at CASSCF level are usually underestimated with respect to the experimental ones.[44−46] In fact, the dynamical electronic correlation plays a crucial role in the description of the energy separation, and this differential effect needs to be taken into account to obtain a quantitative agreement with the experimental J values.[45] These effects can be introduced by means of different approaches.[44] Here, we have chosen to use DDCI calculations, which have been proven to successfully reproduce the experimental J values in many molecular and solid state magnetic systems.[46−52] For the cost of the DDCI calculations to be reduced, the set of MOs has been truncated using their participation in the description of the energy differences (*difference dedicated* MOs) of the involved states as criteria.[53] Only the orbitals with a participation number larger than a certain threshold are retained. Different truncation thresholds have been employed to verify the impact on the J values. The results reported here have been carried out with only 50% of the MO space. No remarkable effect on J values is observed with larger MO spaces.

Table 1 lists the J and J_{NO} values calculated at CASSCF and DDCI levels for the structures reported for $Cu(hfac)_2L^{Bu}\cdot 0.5C_8H_{18}$ at six different temperatures. The values at CASSCF

DOI: 10.1021/acs.inorgchem.5b00794
Inorg. Chem. 2015, 54, 6891−6899

Table 1. Exchange Coupling Constants J (cm^{-1}) within Spin Triads for $Cu(hfac)_2L^{Bu}\cdot 0.5C_8H_{18}$ at CASSCF and DDCI Levels Using the Quartet CASSCF(3/3) MOs and the Doublet CASSCF(3/3) MOs

	CASSCF		DDCI			
			Q_2 MOs		D_2 MOs	
T (K)	J	J_{NO}	J	J_{NO}	J	J_{NO}
100	−37.7	2.6	−145.3	0.2	−167.4	1.2
125	−5.9	0.8	−23.5	0.3	−31.4	0.4
145	2.0	0.2	5.1	−0.1	3.5	−0.1
155	3.1	0.2	9.0	−0.1	9.4	−0.4
175	2.9	0.1	8.3	0.0	9.4	−0.3
295	3.1	0.1	8.7	−0.1	8.0	0.6

levels are comparable to those reported by Vancoillie et al.[37] from CASSCF(11/12) calculations on the DFT-optimized structures of two models of relative compound $Cu(hfac)_2L^{Pr}$. Also, in that case, the CASSCF $|J|$ values were underestimated with respect to the experimental values. As mentioned above, the absolute values of the magnetic coupling constants are significantly enhanced when the electronic correlation effects are taken into account, and it is possible to consider the values obtained at the DDCI level as our best estimate of the couplings in the system. As expected, the dominant interaction is the coupling between Cu and NO groups, J, showing a gradual increase if the ferromagnetic nature as the temperature rises. In the transition region, the Cu 3d orbital is oriented in a similar way as at high temperature (Figure 3 shows the active orbitals at 145 K), and J is ferromagnetic. The coupling between the NO groups (J_{NO}) is rather weak at all temperatures. The impact of the MO set employed in the DDCI calculations is not significant, although the antiferromagnetic character of the magnetic interaction is slightly enhanced at low temperature when the doublet state orbitals are used. However, as will be shown below, these small differences have no consequence on the simulated thermal dependence of the effective magnetic moment curve. In this context, it is worth noting that the reliability of the DDCI calculated J values has been proven to be larger for antiferromagnetic interactions than for ferromagnetic ones, where this approach usually provides underestimated values of the magnetic coupling constants compared to the experimental estimates. This can be partially ascribed to limitations inherent to the method[54] but also to known difficulties of the fitting procedure to provide a unique set of magnetic parameters for compounds with ferromagnetic ground states.[55,56] In the case of $Cu(hfac)_2L^{Bu}\cdot 0.5C_8H_{18}$, the intracluster interactions at high-temperature are ferromagnetic in nature, and our estimates could represent a low-limit of the real values. However, as will be shown, the $\mu_{eff}(T)$ curve is more sensitive to the presence of non-negligible intercluster exchange couplings than to the absolute value of J.

3.2. Evaluation of the Intercluster Magnetic Coupling.

The presence of a non-negligible interaction between the chains has been explored by means of theoretical calculations on a fragment modeling the short contacts between two neighboring chains (Figure 4). The coordinates of all of the atoms have been extracted from the X-ray data structures at 100 and 295 K. The fragment contains two unpaired electrons distributed in two magnetic orbitals. The coupling can be evaluated from the singlet−triplet energy difference, $2J' = E(S) - E(T)$, using DDCI(2/2) calculations on the basis of the triplet CASSCF(2/2) molecular orbitals. The terminal NO groups are separated by a distance of 3.94 Å at 100 K and 4.09 Å at 295 K, and their relative orientation favors a direct interaction between the NO π orbitals, as shown in Figure 5.

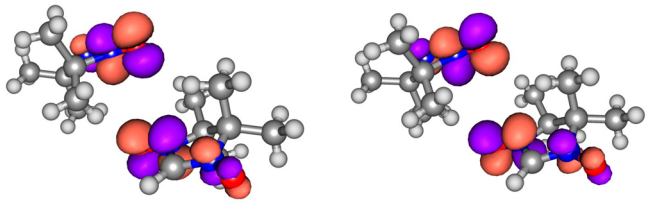

Figure 5. Active magnetic orbitals controlling the interchain magnetic coupling at 100 K (left) and 295 K (right).

Then, the interchain interaction is derived from the coupling through these terminal NO groups, being antiferromagnetic in nature with a J' value of -8.3 cm^{-1} at 100 K and -4.4 cm^{-1} at 295 K (Table 2). The drop in the coupling is consistent with

Table 2. Interchain Magnetic Coupling in for $Cu(hfac)_2L^{Bu}\cdot 0.5C_8H_{18}$ at 100 and 295 K Calculated at the DDCI(2/2) Level with Key Distances and Angles Also Given

T (K)	J' (cm^{-1})	NO···NO (Å)	NO···ON (Å)	NO···NO (deg)
100	−8.3	3.94	4.01	96.1
295	−4.4	4.09	4.22	92.7

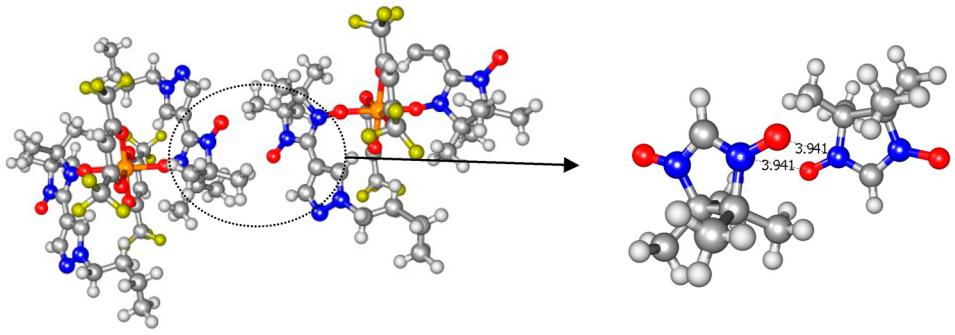

Figure 4. (left) Representation of the short-contact region between the chains in $Cu(hfac)_2L^{Bu}\cdot 0.5C_8H_{18}$ at 100 K and (right) fragment employed to calculate the intercluster magnetic coupling. Cu, O, N, C, F, and H are represented by orange, red, blue, dark gray, yellow, and light gray, respectively.

DOI: 10.1021/acs.inorgchem.5b00794
Inorg. Chem. 2015, 54, 6891−6899

the increase in the separation between the NO groups. The DDCI J' value at 100 K is in agreement with previously reported calculations based on a broken-symmetry density functional approach[14] with J' values ranging from −7.57 to −9.55 cm^{-1} depending on the choice of the exchange-correlation functional and atom basis functions.

Remarkably, Table 2 shows that intercluster exchange coupling constant J' noticeably (by roughly a factor of 2) changes with temperature upon transitioning from a strongly to weakly coupled spin state. At the same time, even at high temperatures, the magnitude of coupling remains relatively high (−4.4 cm^{-1}). Note that this value of interchain coupling becomes comparable to the J value *within* spin triads. This means that in the weakly coupled state there is no dominating exchange coupling, and the spin level structure becomes, figuratively speaking, a "continuum" of states condensed within ∼10−20 cm^{-1}. Such information is vital for interpretation of spin dynamics and relaxation in photoinduced WS states at low temperatures. For instance, the unusual self-decelerating character of structural relaxation from photoinduced WS state to the ground SS state may have this "continuum of states" as a major cause, as was proposed earlier.[17,19] High values of J' in the WS state theoretically rationalized in this work support this explanation. In addition, intercluster exchange coupling was assumed to be a major mechanism averaging EPR signals of individual spins at high temperatures,[9] yet this was grounded only on the assumption that J' is approximately the same in the SS and WS states. Herein, we provide solid support that even though J' drops by a factor of ∼2 at high temperature, the absolute value still remains high enough on the EPR energy scale, and thus readily leads to the exchange narrowing observed experimentally.

3.3. Simulation of the Thermal Dependence of the Effective Magnetic Moment. To verify the reliability of our theoretical results, we have simulated the thermal dependence of the effective magnetic moment using the values obtained at the DDCI level. The molar magnetic susceptibility and effective magnetic moment calculated per $\{Cu(hfac)_2L^R\}$ fragment (ignoring diamagnetic contribution) are given by

$$\chi = 0.5\chi_{triad} + 0.5\chi_{mono}$$
$$\mu_{eff} = \sqrt{3kT\chi/(N\mu_B^2)} \quad (3)$$

where χ_{triad} is the molar susceptibility of the NO-Cu-ON spin triad in the CuO_6 sites, and χ_{mono} corresponds to the molar susceptibility of the Cu ions ($S = 1/2$) in the CuO_4N_2 sites

$$\chi_{mono} = \frac{N\mu_B^2 g_{Cu-mono}^2}{3kT} S(S+1) + N\alpha$$
$$\chi_{triad} = \frac{N\mu_B^2}{3kT} \frac{1.5g_A^2 e^{-E(D_2)/kT} + 1.5g_B^2 e^{-E(D_1)/kT} + 15g_C^2 e^{-E(Q_2)/kT}}{2e^{-E(D_1)/kT} + 2e^{-E(D_2)/kT} + 4e^{-E(Q_2)/kT}} + N\alpha$$
$$g_A = (4g_{NO} - g_{Cu})/3, \quad g_B = g_{Cu}, \quad g_C = (2g_{NO} + g_{Cu})/3 \quad (4)$$

g_{Cu} and g_{NO} refer to the g factors of copper and nitroxide within a spin triad, respectively, and $g_{Cu-mono}$ referes to the copper in the one-spin unit. $N\alpha$ corresponds to the temperature-independent paramagnetism (TIP). Replacing the energies of the three magnetic states by eq 2, the molar susceptibility of the triad reads as

$$\chi_{triad} = \frac{N\mu_B^2}{3kT} \frac{1.5g_A^2 e^{-3J/kT} + 1.5g_B^2 e^{-J-2J_{NO}/kT} + 15g_C^2}{2e^{-3J/kT} + 2e^{-J-2J_{NO}/kT} + 4} + N\alpha \quad (5)$$

Figure 6 shows the simulations of the thermal dependence of the effective magnetic moment obtained with the ab initio J and

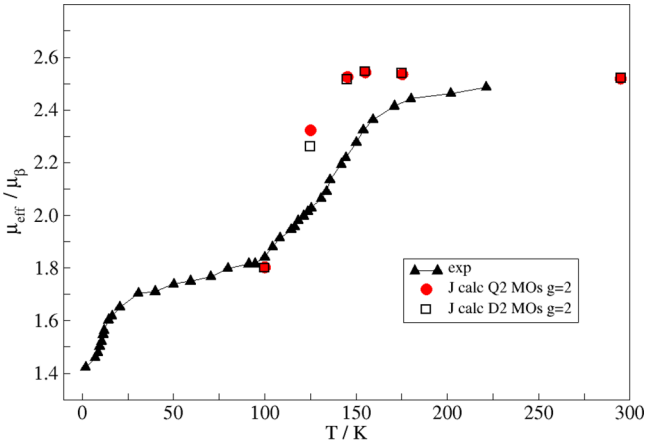

Figure 6. Simulated thermal dependence of the magnetic moment with the calculated J values obtained with quartet MOs (red circles) and doublet MOs (open black squares), both with $g_A = g_B = g_C = 2$ and $g_{Cu-mono} = 2.15$.

J_{NO} values and the g factors as $g_A = g_B = g_C = 2$ and $g_{Cu-mono} = 2.15$. The simulations reproduce the general trend of the experimental $\mu_{eff}(T)$ curve (powder sample, data taken from ref 10) independently of the set of J values employed (values resulting from the calculations using the quartet or the doublet MOs). Hereafter, only the simulations using the J values obtained with the quartet CASSCF(3/3) MOs are discussed.

To verify the impact of the values given to the g factors, the simulation was also performed using the $g_{Cu} = 2.15$ and $g_{NO} = 2.007$ values suggested by Fedin et al.,[57] leading to $g_A = 2.15$, $g_B = 1.96$, and $g_C = 2.05$ in eq 5. As shown in Figure 7 (open red circles), the simulation does not change significantly, showing almost the same trend as with $g = 2$.

The intercluster exchange interaction can be also taken into account by means of the mean field approximation as follows

$$\mu^2 = \mu_{eff}^2 \Big/ \left[1 - \frac{2z'J'}{3kT} \frac{\mu_{eff}^2}{g_{eff}'^2}\right] \quad (6)$$

where z' is the cluster lattice coordination number ($z' = 2$), and J' is the value of the intercluster coupling constant. Veber et al.[11] have reported a satisfactory fit of the thermal dependence of μ_{eff} at $T < 50$ K with $z'J' = -10$ cm^{-1} and $g'_{eff} = 1.96$. Figure 7 shows the plot obtained when this effect is also included in the simulation of the $\mu_{eff}(T)$ curve using the $z'J'$ value proposed by Veber (open diamonds) and the $z'J'$ value resulting from our ab initio calculations for the 100 K structure (filled diamonds). Both sets are comparable, showing a nice improvement in the transition region with respect to the simulations obtained without the intercluster exchange.

3.4. Molecular-Level Interpretation of the Magnetic Data. Although the simulation shown in Figure 7, including the effect of interchain interactions, presents reasonable agreement with the experimental curve, closer inspection indicates that even the best of the fitted curve does not correctly reproduce

DOI: 10.1021/acs.inorgchem.5b00794
Inorg. Chem. 2015, 54, 6891−6899

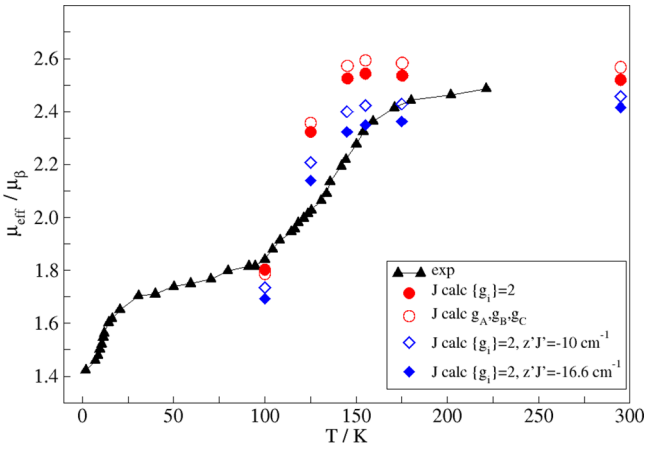

Figure 7. Simulated thermal dependence of the magnetic moment with the calculated J values using the quartet MOs and different sets of g values: $g_A = g_B = g_C = 2$ and $g_{Cu-mono} = 2.15$ (filled red circles), $g_A = 2.15$, $g_B = 1.96$, and $g_C = 2.05$ and $g_{Cu-mono} = 2.15$ (open red circles). The diamonds correspond to the simulation, taking into account the intercluster exchange interactions, open diamonds with $z'J' = -10$ cm^{-1} and $g'_{eff} = 1.96$ as suggested by Veber et al.[11] and the filled diamonds using the ab initio intercluster exchange interaction at 100 K, $J' = -8.3$ cm^{-1}, $z' = 2$, and $g'_{eff} = 1.96$.

the slope of the experimental $\mu_{eff}(T)$ curve in the transition region. This could be related to missing effects in the model employed to simulate the magnetic data or could provide an alternative view of the experimentally obtained crystal structures and their interpretation.

In this sense, a distinct interpretation of gradual changes of the magnetic moment in breathing crystals compared to the one based on literal interpretation of XRD data was also proposed.[10,58] It was assumed that it is possible to have an average of low- (LT) and high-temperature (HT) structures in the transition region in such a way that the magnetic moment changes with temperature just because the percentage of each phase also changes. In this scenario, the X-ray structures provided for the transition temperatures are not real structures but represent an average structure resulting from this changing mixture of LT and HT structures (this agrees well with the observed broadening of the diffraction peaks in the transition region). The gradual magnetostructural transition, then, can be interpreted as the result of the gradual change of the percentage of the HT (or LT) phase instead of a gradual change of the structure. Obviously, the model of two coexisting phases in a ratio changing with temperature does not exclude additional effects having minor impact on the transition, such as the thermal shrinking of bonds in each phase also found in nonbreathing analogues of breathing crystals.[18,59]

With this idea in mind, it is possible to reanalyze our results. Table 3 lists the X-ray diffraction data for the Cu−O distances of the CuO_6 unit in the spin triad of $Cu(hfac)_2L^{Bu}{\cdot}0.5C_8H_{18}$ at different temperatures.

If these geometric parameters do not correspond to real configurations but rather to an average of the LT and HT structures, we need to estimate the weight fractions (w) of the LT phase at each temperature. We can consider that for each temperature T in the transition region (125−175 K), the Cu−O distances d_T just correspond to the average of the distances in the LT and HT phases. The percentage of LT phase present at each temperature is w, and $(1 - w)$ for the HT phase such that

$$d_T = wd_{LT} + (1 - w)d_{HT} \quad (7)$$

The w values can be obtained by solving the redundant system of equations for each temperature using the least-squares method (Table 3), considering the structures at 100 and 295 K as the LT and HT phases, respectively. Using the w values obtained in this manner, it is possible to correctly reproduce the temperature dependence of the Cu−O distances in the transition region (between 100 and 295 K); the highest relative error found for the estimated Cu−O d_T distances (eq 7) is 0.9% and corresponds to $Cu-O_{hfac2}$ distances, as shown in Table 3 and Figure 8.

Now, the molar magnetic susceptibility of the spin triad (χ_{triad}) also depends on the weight fraction w and has the form[58]

$$\chi_{triad} = w\chi_{LT} + (1 - w)\chi_{HT} \quad (8)$$

where χ_{LT} and χ_{HT} are the molar magnetic susceptibility of the LT and HT phases, respectively. Using the w fractions and the calculated J and J_{NO} values for the 100 and 295 K structures, a nice improvement in the simulation in the transition region is obtained, as shown in Figure 9. This suggests that during gradual transitions in breathing crystals the two phases (LT and HT) coexist, and then the X-ray structures for this region refer to the average of the LT and HT structures at different percentages depending on the temperature. At 100 K, the w value employed in the simulation is $w = 0.85$ instead of 1. This deviation indicates that a better agreement could be possible using a lower temperature structure as LT phase in eq 7 or even using additional structural parameters, such as bond and torsion angles. However, despite its approximate nature, the weighting

Table 3. (top) Cu−O Distances (Å) for Each X-ray Structure of $Cu(hfac)_2L^{Bu}{\cdot}0.5C_8H_{18}$ and Weight Fractions of the Low Temperature Phase and (bottom) Cu−O Distances (d_T, Å) for Structures in the Transition Region Estimated as an Average of the Corresponding Distances in the LT and HT Structures (eq 7) with Relative Error (%) in Parentheses

	X-ray data					
	100 K = LT	125 K	145 K	155 K	175 K	295 K = HT
$Cu-O_{NO}$	2.034	2.122	2.189	2.260	2.307	2.352
$Cu-O_{hfac1}$	1.998	1.993	1.981	1.969	1.965	1.960
$Cu-O_{hfac2}$	2.201	2.108	2.060	2.011	1.990	1.971
w	1	0.6812	0.4702	0.2495	0.1214	0
			average LT and HT structures			
$Cu-O_{NO}$		2.135 (0.63)	2.202 (0.62)	2.273 (0.56)	2.313 (0.28)	
$Cu-O_{hfac1}$		1.986 (0.36)	1.978 (0.16)	1.969 (0.02)	1.965 (0.02)	
$Cu-O_{hfac2}$		2.128 (0.93)	2.079 (0.93)	2.028 (0.86)	1.999 (0.45)	

DOI: 10.1021/acs.inorgchem.5b00794
Inorg. Chem. 2015, 54, 6891−6899

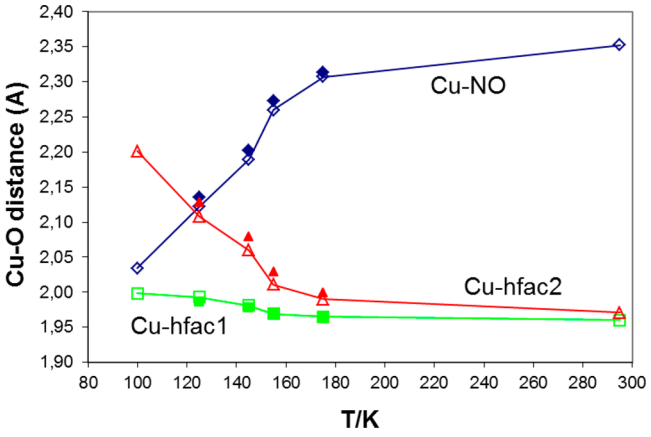

Figure 8. Comparison between the reported X-ray Cu−O distances (Å) in the spin triad (filled symbols) and the Cu−O distances resulting from the average of the LT and HT structures in the transition region (open symbols).

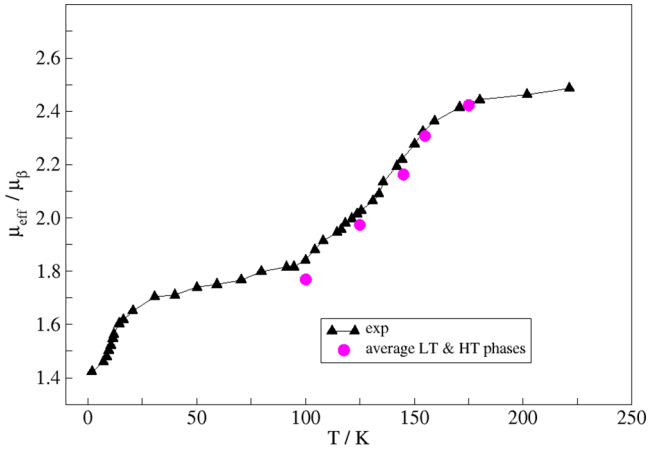

Figure 9. Simulated temperature dependence of the magnetic moment with weight fractions of the LT and HT phases at each temperature, including interchain interactions: $g_A = g_B = g_C = 2$, $g_{Cu-mono} = 2.15$, $z'J' = -16.6$ cm^{-1}, $g'_{eff} = 1.96$ and TIP = 1.5×10^{-3} cm^3 mol^{-1}.

coefficients are useful for illustrating the presence of two coexisting phases in the system. Note that this theoretical finding is in perfect agreement with recent FTIR study of breathing crystals,[22] where the experimental evidence for the coexistence of LT and HT structures during gradual magneto-structural transition was provided. Note also that, in addition to new structural insights, the model of two coexisting phases allows good fitting of $\mu_{eff}(T)$ dependence (Figure 9) as the model of effective uniform triads.[11]

4. CONCLUSIONS

The intracluster and intercluster magnetic exchange interactions present in the complex $Cu(hfac)_2L^{Bu}{\cdot}0.5C_8H_{18}$, and their dependence on temperature, have been analyzed by means of DDCI calculations. In the spin triads, the dominant exchange interaction between Cu center and nitroxide groups J is strongly antiferromagnetic at low temperature and becomes ferromagnetic when the temperature increases. This behavior is due to the change of the relative orientation of the active π nitroxide and 3d Cu orbitals promoted by the temperature-driven structural distortion of the triad Cu center. The interaction between the nitroxide π orbitals is negligible across the range of temperatures. The intercluster coupling J' is antiferromagnetic in nature, which is favored by the 1D packing of the polymeric chains. This packing allows for an efficient π pathway between NO groups belonging to different chains. J' is also strongly affected by temperature; its value drops by a factor of 2 at high temperature. This interaction is comparable in magnitude to the J coupling within spin triads, and then no dominant exchange coupling exists at high temperature. This is of crucial importance for interpreting the spin dynamics and relaxation in photoinduced WS states at low temperature as well as the averaging of the EPR signals at high temperature.

The simulation of the $\mu_{eff}(T)$ curve using the calculated intracluster J values for each temperature correctly reproduces the general characteristics of the gradual magnetostructural transition found in this breathing crystal, in particular when the intercluster coupling is also taken into account. The simulation can be quantitatively improved considering that the spin triads can be found in one of two geometries (LT or HT phase) characterized by different magnetic moment and that the ratio between these phases changes with temperature. The magneto-structural transition can then be interpreted as the result of the gradual change of the percentage of LT and HT phases instead of the gradual change of structure. The conclusions here, referring to $Cu(hfac)_2L^{Bu}{\cdot}0.5C_8H_{18}$, are expected to be transferable to the rest of the $Cu(hfac)_2L^{R}$ breathing crystals presenting with a gradual magnetostructural transition.

As follows from recent studies on breathing crystals exhibiting gradual magnetostructural transitions, including the present study, available experimental techniques allow only for effective values of exchange couplings to be spatial or temporal averages of coexisting phases.[9] Thus, experimental determination of these exchange couplings becomes impossible without the involvement of cutting-edge quantum chemistry calculations. Therefore, the development and application of new approaches for precise calculations of exchange couplings in breathing crystals $Cu(hfac)_2L^{R}$, in this work as well as in the future, is required for qualitative and quantitative characterization of magnetic anomalies in this type of switchable molecular magnet.

■ ASSOCIATED CONTENT

Supporting Information

Listings of Cartesian coordinates for the models employed in the DDCI calculations of the intracluster and intercluster magnetic coupling constants. The Supporting Information is available free of charge on the ACS Publications website at DOI: 10.1021/acs.inorgchem.5b00794.

■ AUTHOR INFORMATION

Corresponding Author

*E-mail: calzado@us.es.

Notes

The authors declare no competing financial interest.

■ ACKNOWLEDGMENTS

The authors acknowledge the financial support of the Universidad de Sevilla (Spain). The Supercomputing Team of the Centro Informático Científico de Andalucía (CICA) is deeply acknowledged for technical support. J.J. thanks Rennes Métropole for the grant allowing her 3-month stay in Sevilla. M.V.F. thanks RFBR (14-03-00224) and the RF President's Grant (MD-276.2014.3) for financial support.

DOI: 10.1021/acs.inorgchem.5b00794
Inorg. Chem. 2015, 54, 6891−6899

REFERENCES

(1) Themed issue: Molecule-based magnets.*Chem. Soc. Rev.* **2011**, *40*, 3053−3368.
(2) *Molecular Magnetism: From Molecular Assemblies to the Devices*; Coronado, E., Delhaès, P., Gatteschi, D., Miller, J. S., Eds.; Nato ASI Series, E: Applied Sciences; Kluwer Academic Publisher: Dordrecht, The Netherlands, Vol. *321*, 1996.
(3) Gatteschi, D.; Sessoli, R.; Villain, J. *Molecular Nanomagnets*; Oxford University Press, 2006.
(4) Dei, A.; Gatteschi, D. *Angew. Chem., Int. Ed.* **2011**, *50*, 11852−11858.
(5) Mannini, M.; Pineider, F.; Danieli, C.; Totti, F.; Sorace, L.; Sainctavit, Ph.; Arrio, M.-A.; Otero, E.; Joly, L.; Cezar, J. C.; Cornia, A.; Sessoli, R. *Nature* **2010**, *468*, 417−421.
(6) *Spin-Crossover Materials: Properties and Applications*, 1st ed.; Halcrow, M. A., Ed.; John Wiley & Sons, Ltd., 2013.
(7) *Spin Crossover in Transition Metal Compounds*, Vols. I-III; Gutlich, P., Goodwin, H. A., Eds.; Topics in Current Chemistry ; Springer-Verlag: Berlin/Heidelberg/New York, 2004; pp 233−235.
(8) Ovcharenko, V. I., Bagryanskaya, E. G. In *Spin-Crossover Materials: Properties and Applications*, 1st ed., Halcrow, M. A., Ed.; John Wiley & Sons, Ltd., 2013; pp 239−280.
(9) Fedin, M. V.; Veber, S. L.; Bagryanskaya, E. G.; Ovcharenko, V. I. *Coord. Chem. Rev.* **2015**, *289*−*290*, 341−356.
(10) Ovcharenko, V. I.; Romanenko, G. V.; Maryunina, K. Y.; Bogomyakov, A. S.; Gorelik, E. V. *Inorg. Chem.* **2008**, *47*, 9537−9552.
(11) Veber, S. L.; Fedin, M. V.; Potapov, A. I.; Maryunina, K. Y.; Romanenko, G. V.; Sagdeev, R. Z.; Ovcharenko, V. I.; Goldfarb, D.; Bagryanskaya, E. G. *J. Am. Chem. Soc.* **2008**, *130*, 2444−2445.
(12) Fedin, M.; Ovcharenko, V.; Sagdeev, R.; Reijerse, E.; Lubitz, W.; Bagryanskaya, E. *Angew. Chem., Int. Ed.* **2008**, *47*, 6897−6899.
(13) Fedin, M. V.; Veber, S. L.; Romanenko, G. V.; Ovcharenko, V. I.; Sagdeev, R. Z.; Klihm, G.; Reijerse, E.; Lubitz, W.; Bagryanskaya, E. G. *Phys. Chem. Chem. Phys.* **2009**, *11*, 6654−6663.
(14) Fedin, M. V.; Veber, S. L.; Maryunina, K. Y.; Romanenko, G. V.; Suturina, E. A.; Gritsan, N. P.; Sagdeev, R. Z.; Ovcharenko, V. I.; Bagryanskaya, E. G. *J. Am. Chem. Soc.* **2010**, *132*, 13886−13891.
(15) Veber, S. L.; Fedin, M. V.; Maryunina, K. Y.; Potapov, A.; Goldfarb, G.; Reijerse, E. W.; Lubitz, W.; Sagdeev, R. Z.; Ovcharenko, V. I.; Bagryanskaya, E. G. *Inorg. Chem.* **2011**, *50*, 10204−10212.
(16) Romanenko, G. V.; Maryunina, K. Y.; Bogomyakov, A. S.; Sagdeev, R. Z.; Ovcharenko, V. I. *Inorg. Chem.* **2011**, *50*, 6597−6609.
(17) Fedin, M. V.; Maryunina, K. Y.; Sagdeev, R. Z.; Ovcharenko, V. I.; Bagryanskaya, E. G. *Inorg. Chem.* **2012**, *51*, 709−717.
(18) Tretyakov, E. V.; Tolstikov, S. E.; Suvorova, A. O.; Polushkin, A. V.; Romanenko, G. V.; Bogomyakov, A. S.; Veber, S. L.; Fedin, M. V.; Stass, D. V.; Reijerse, E.; Lubitz, W.; Zueva, E. M.; Ovcharenko, V. I. *Inorg. Chem.* **2012**, *51*, 9385−9394.
(19) Fedin, M. V.; Bagryanskaya, E. G.; Matsuoka, H.; Yamauchi, S.; Veber, S. L.; Maryunina, K. Y.; Tretyakov, E. V.; Ovcharenko, V. I.; Sagdeev, R. Z. *J. Am. Chem. Soc.* **2012**, *134*, 16319−16326.
(20) Barskaya, I. Y.; Tretyakov, E. V.; Sagdeev, R. Z.; Ovcharenko, V. I.; Bagryanskaya, E. G.; Maryunina, K. Y.; Takui, T.; Sato, K.; Fedin, M. V. *J. Am. Chem. Soc.* **2014**, *136*, 10132−10138.
(21) Kaszub, W.; Marino, A.; Lorenc, M.; Collet, E.; Bagryanskaya, E. G.; Tretyakov, E. V.; Ovcharenko, V. I.; Fedin, M. V. *Angew. Chem., Int. Ed.* **2014**, *53*, 10636−10640.
(22) Veber, S. L.; Suturina, E. A.; Fedin, M. V.; Boldyrev, K. N.; Maryunina, K. Y.; Sagdeev, R. Z.; Ovcharenko, V. I.; Gritsan, N. P.; Bagryanskaya, E. G. *Inorg. Chem.* **2015**, *54*, 3446−3455.
(23) Caneschi, A.; Chiesi, P.; David, L.; Ferraro, F.; Gatteschi, D.; Sessoli, R. *Inorg. Chem.* **1993**, *32*, 1445−1453.
(24) Lanfranc de Panthou, F.; Belorizky, E.; Calemczuk, R.; Luneau, D.; Marcenat, C.; Ressouche, E.; Turek, P.; Rey, P. *J. Am. Chem. Soc.* **1995**, *117*, 11247−11253.
(25) Inoue, K.; Iwahori, F.; Iwamura, H. *Chem. Lett.* **1998**, 737−738.
(26) Iwahori, F.; Inoue, K.; Iwamura, H. *Mol. Cryst. Liq. Cryst.* **1999**, *334*, 533−538.
(27) Baskett, M.; Lahti, P. M.; Paduan-Filho, A.; Oliveira, N. F. *Inorg. Chem.* **2005**, *44*, 6725−6735.
(28) Baskett, M.; Paduan-Filho, A.; Oliveira, N. F.; Chandrasekaran, A.; Mague, J. T.; Lahti, P. M. *Inorg. Chem.* **2011**, *50*, 5060−5074.
(29) Allão Cassaro, R. A.; Baskett, M.; Lahti, P. M. *Polyhedron* **2013**, *64*, 231−237.
(30) Hirel, C.; Li, L.; Brough, P.; Vostrikova, K.; Pecaut, J.; Mehdaoui, B.; Bernard, M.; Turek, P.; Rey, P. *Inorg. Chem.* **2007**, *46*, 7545−7552.
(31) Setifi, F.; Benmansour, S.; Marchivie, M.; Dupouy, G.; Triki, S.; Sala-Pala, J.; Salaun, J. Y.; Gomez-Garcia, C. J.; Pillet, S.; Lecomte, C.; Ruiz, E. *Inorg. Chem.* **2009**, *48*, 1269−1271.
(32) Okazawa, A.; Hashizume, D.; Ishida, T. *J. Am. Chem. Soc.* **2010**, *132*, 11516−11524.
(33) Okazawa, A.; Ishida, T. *Inorg. Chem.* **2010**, *49*, 10144−10147.
(34) Morozov, V. A. *Russ. Chem. Bull.* **2013**, *61*, 1837.
(35) Morozov, V. A. *Phys. Chem. Chem. Phys.* **2013**, *15*, 9931−9939.
(36) Morozov, V. A.; Lukzen, N. N.; Ovcharenko, V. I. *J. Phys. Chem. B* **2008**, *112*, 1890−1893.
(37) Vancoillie, S.; Rulísek, L.; Neese, F.; Pierloot, K. *J. Phys. Chem. A* **2009**, *113*, 6149−6157.
(38) Streltsov, S. V.; Petrova, M. V.; Morozov, V. A.; Romanenko, G. V.; Anisimov, V. I.; Lukzen, N. N. *Phys. Rev. B* **2013**, *87*, 024425.
(39) (a) Miralles, J.; Daudey, J.-P.; Caballol, R. *Chem. Phys. Lett.* **1992**, *198*, 555−562. (b) Miralles, J.; Castell, O.; Caballol, R.; Malrieu, J.-P. *Chem. Phys.* **1993**, *172*, 33−43.
(40) (a) Widmark, P.-O.; Malmqvist, P.-A.; Roos, B. O. *Theor. Chim. Acta* **1990**, *77*, 291−306. (b) Roos, B. O.; Lindh, R.; Malmqvist, P.-Å.; Veryazov, V.; Widmark, P. O. *J. Phys. Chem. A* **2004**, *108*, 2851−2857.
(41) The calculations have been performed with the "old" ANO-RCC basis set for C atoms, which contained an error in the contraction scheme reported by the MOLCAS team during the preparation of the manuscript. Prior to submission, a new set of calculations was performed with the corrected carbon ANO-RCC basis, and any changes are observed in the calculated *J* values.
(42) Aquilante, F.; de Vico, L.; Ferr, N.; Ghigo, G.; Malmqvist, P.-A.; Pedersen, T.; Pitonak, M.; Reiher, M.; Roos, B. O.; Serrano-Andrés, L.; Urban, M.; Veryazov, V.; Lindh, R. *J. Comput. Chem.* **2010**, *31*, 224−247.
(43) CASDI program: Ben Amor, N.; Maynau, D. *Chem. Phys. Lett.* 1998, *286*, 211−220, package developed at the Laboratoire de Chimie et Physique Quantiques, Université Paul Sabatier: Toulouse (France).
(44) Malrieu, J. P.; Caballol, R.; Calzado, C. J.; de Graaf, C.; Guihery, N. *Chem. Rev.* **2014**, *114*, 429−492.
(45) (a) Calzado, C. J.; Cabrero, J.; Malrieu, J.-P.; Caballol, R. J. *Chem. Phys.* **2002**, *116*, 2728−2747. (b) Calzado, C. J.; Cabrero, J.; Malrieu, J.-P.; Caballol, R. *J. Chem. Phys.* **2002**, *116*, 3985−4000. (c) Calzado, C. J.; Angeli, C.; Taratiel, D.; Caballol, R.; Malrieu, J.-P. *J. Chem. Phys.* **2009**, *131*, 044327.
(46) (a) Oms, O.; Rota, J. B.; Norel, L.; Calzado, C. J.; Rousseliere, H.; Train, C.; Robert, V. *Eur. J. Inorg. Chem.* **2010**, 5373−5378. (b) Bandeira, N. A. G.; Maynau, D.; Robert, V.; Le Guennic, B. *Inorg. Chem.* **2013**, *52*, 7980−7986. (c) Rota, J. B.; Calzado, C. J.; Train, C.; Robert, V. *J. Chem. Phys.* **2010**, *132*, 154702. (d) Vérot, M.; Rota, J. B.; Kepenekian, K.; Le Guennic, B.; Robert, V. *Phys. Chem. Chem. Phys.* **2011**, *13*, 6657. (e) Aronica, C.; Chastanet, G.; Pilet, G.; Le Guennic, B.; Robert, V.; Wernsdorfer, W.; Luneau, D. *Inorg. Chem.* **2007**, *46*, 6108−6119. (f) Costa, J. S.; Bandeira, N. A. G.; Le Guennic, B.; Robert, V.; Gamez, P.; Chastanet, G.; Ortiz-Frade, L.; Gasque, L. *Inorg. Chem.* **2011**, *50*, 5696−5705. (g) Le Guennic, B.; Ben Amor, N.; Maynau, D.; Robert, V. *J. Chem. Theory Comput.* **2009**, *5*, 1506−1510.
(47) (a) Calzado, C. J.; Sanz, J. F.; Malrieu, J. P. *J. Chem. Phys.* **2000**, *112*, 5158−5167. (b) Calzado, C. J.; Evangelisti, S.; Maynau, D. *J. Phys. Chem. A* **2003**, *107*, 7581−7588.
(48) (a) Casanovas, J.; Illas, F. *J. Chem. Phys.* **1994**, *100*, 8257−8263. (b) Moreira, I. P. R.; Illas, F.; Calzado, C. J.; Sanz, J.; Malrieu, J. P.; Ben Amor, N.; Maynau, D. *Phys. Rev. B* **1999**, *59*, 6593−6596. (c) de Graaf, C.; Moreira, I. P. R.; Illas, F.; Martin, R. L. *Phys. Rev. B* **1999**, *60*,

DOI: 10.1021/acs.inorgchem.5b00794
Inorg. Chem. 2015, 54, 6891−6899

3457−3464. (d) Muñoz, D.; Illas, F.; Moreira, I. P. R. *Phys. Rev. Lett.* **2000**, *84*, 1579−1582.
(49) (a) Cabrero, J.; de Graaf, C.; Bordas, E.; Caballol, R.; Malrieu, J. P. *Chem.—Eur. J.* **2003**, *9*, 2307−2315. (b) Queralt, N.; Taratiel, D.; de Graaf, C.; Caballol, R.; Cimiraglia, R.; Angeli, C. *J. Comput. Chem.* **2008**, *29*, 994−1003.
(50) Suaud, N.; Gaita-Arino, A.; Clemente-Juan, J. M.; Sanchez-Marin, J.; Coronado, E. *J. Am. Chem. Soc.* **2002**, *124*, 15134−15140.
(51) (a) Barone, V.; Cacelli, I.; Ferretti, A.; Monti, S.; Prampolini, G. *J. Chem. Theory Comput.* **2011**, *7*, 699−706. (b) Barone, V.; Cacelli, I.; Ferretti, A.; Monti, S.; Prampolini, G. *Phys. Chem. Chem. Phys.* **2011**, *13*, 4709−4714.
(52) (a) Neese, F. *J. Am. Chem. Soc.* **2006**, *128*, 10213−10222. (b) Liakos, D. G.; Ganyushin, D.; Neese, F. *Inorg. Chem.* **2009**, *48*, 10572−10580. (c) Ganyushin, D.; Gilka, N.; Taylor, P. R.; Marian, C. M.; Neese, F. *J. Chem. Phys.* **2010**, *132*, 144111. (d) McNaughton, R. L.; Roemelt, M.; Chin, J. M.; Schrock, R. R.; Neese, F.; Hoffman, B. M. *J. Am. Chem. Soc.* **2010**, *132*, 8645−8656.
(53) (a) Calzado, C. J.; Malrieu, J.-P.; Cabrero, J.; Caballol, R. *J. Phys. Chem. A* **2000**, *104*, 11636−11643. (b) Miralles, J.; Caballol, R.; Malrieu, J.-P. *Chem. Phys.* **1991**, *153*, 25−37.
(54) Calzado, C. J. Manuscript in preparation.
(55) Schwabe, L.; Haase, W. *J. Chem. Soc., Dalton Trans.* **1985**, 1909−1913.
(56) Calzado, C. J. *Chem.—Eur. J.* **2013**, *19*, 1254−1261.
(57) Fedin, M.; Veber, S.; Gromov, I.; Maryunina, K. Y.; Fokin, S.; Romanenko, G.; Sagdeev, R.; Ovcharenko, V.; Bagryanskaya, E. *Inorg. Chem.* **2007**, *46*, 11405−11415.
(58) Zueva, E. M.; Ryabykh, E. R.; Kuznetsov, A..M. *Russ. Chem. Bull., Int. Ed.* **2009**, *58*, 1654−1662.
(59) Tretyakov, E. V.; Romanenko, G. V.; Veber, S. L.; Fedin, M. V.; Polushkin, A. V.; Tkacheva, A. O.; Ovcharenko, V. I. *Aust. J. Chem.* **2015**, *96*, 970−980.

DOI: 10.1021/acs.inorgchem.5b00794
Inorg. Chem. 2015, 54, 6891−6899